Supplementary material for *New global observations of the terrestrial carbon cycle from GOSAT: Patterns of plant fluorescence with gross primary productivity*

Christian Frankenberg,[1] Joshua B. Fisher,[1] John Worden,[1] Grayson Badgley,[1] Sassan S. Saatchi,[1] Jung-Eun Lee,[1] Geoffrey C. Toon,[1] André Butz,[2] Martin Jung,[3] Akihiko Kuze,[4] and Tatsuya Yokota[5]

[1] *Jet Propulsion Laboratory, California Institute of Technology, Pasadena, USA.*

[2] *Karlsruhe Institute of Technology, Institute for Meteorology and ClimateResearch, Germany*

[3] *Biogeochemical Model-Data Integration Group, Max Planck Institute for Biogeochemistry, Jena, Germany.*

[4] *Japan Aerospace Exploration Agency, Sengen 2-2-1, Tsukuba 305-8505, Japan.*

[5] *National Institute for Environmental Studies, Onogawa 16-2, Tsukuba 305-8506, Japan.*

(Dated: August 17, 2011)

In the supplementary material, Section I discusses the GOSAT specific fluorescence retrieval as well as post-processing in detail. Section II describes a crucial step towards accurate fluorescence retrievals from GOSAT as we detect and correct a zero-level offset in GOSAT O_2A-band spectra. The correction method as well as its impact on the fluorescence signal is outlined in detail and more instrument specific aspects discussed. Section III provides an overview and rationale on accuracy and precision estimates. Section IV describes the computation of $\overline{F_S}$, section V the complex relationship of fluorescence yield with GPP and LUE. In section VI, we describe MODIS data handling and section VII provides few ancillary plots to support conclusions of the main document.

I. GOSAT FLUORESCENCE FITS

GOSAT records high-resolution O_2A-band spectra in two orthogonal polarization directions, denoted S and P. The spectral resolution is determined by the maximum optical path difference of the system (2.5 cm) and the field-of-view (7.9 mrad, half angle). We use an analytical instrument line-shape model (sinc convolved with a box-function accounting for a small misalignment factor [5]).

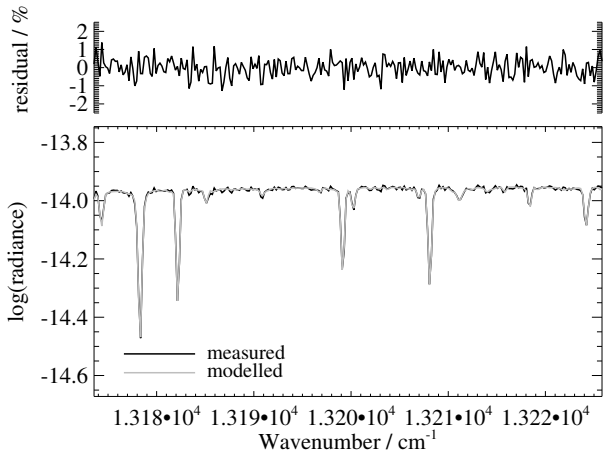

FIG. S1. Exemplary fluorescence fit of a single GOSAT spectrum (S-polarization) in the 755 nm region on May 17, 2010 (lat=34.5697°, lon=2.3986°, SZA=23.31°, SNR ≈ 190). Wavenumbers are used as x-axis since we are dealing with an FTS system. Fit results: reduced χ^2: 1.089; $F_s^{rel} = 1.41 \pm 0.65\%$ (fluorescence signal as relative fraction of the continuum signal, see Frankenberg *et al.* [2] for details).

Figures S1–S2 show examples of typical fluorescence fits in two wavelength regions, using the retrieval as described in Frankenberg *et al.* [2]. The window around 772 nm contains one very strong Fraunhofer line, which is the focus of retrievals performed by Joiner *et al.* [4]. We have fitted a larger window and also model the weak O_2 lines in order to minimize interferences due to the sinc-type instrumental line-shape. In contrast to Joiner *et al.* [4], we don't have to invoke any additional unexplained spectral features as our fit residuals are within the expected noise levels (i.e. the reduced χ^2 is around 1) and we do not observe large systematic residuals. The O_2 lines are used to retrieve an independent estimate for surface pressure using an IMAP-DOAS approach [3]. Deviations of the retrieved surface pressure p_s from ECMWF surface pressure are subsequently used as a cloud filter. In the retrieval, we allow for a spectral shift of both Fraunhofer lines and telluric O_2 lines independently.

For each GOSAT ground-pixel, 4 retrievals are performed independently: 2 retrieval windows

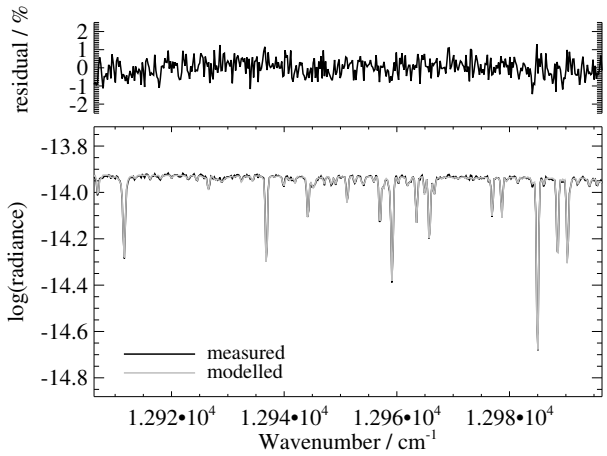

FIG. S2. As Fig. S1 but for the 772 nm retrieval window. In contrast to the 755 nm window, weak O_2 lines are present in this window and used to retrieve surface pressure in addition to fluorescence. Fit results: reduced χ^2: 0.963; $F_s^{rel} = 1.68 \pm 0.47\%$; surface pressure: 929.9 hPa (ECMWF prior: 910.2 hPa)

TABLE S1. Filter criteria for GOSAT fluorescence retrievals.

Quantity	criterion
reduced χ^2	$0.9 < \chi^2 < 1.1$
retr. surface pressure p_s	$0.9 \cdot p_s^{ECMWF} < p_s < 1.1 \cdot p_s^{ECMWF}$
average signal level / $(10^{-7}\mathrm{Wcm^{-2}sr^{-1}cm^{-1}})$	$1.5 < \overline{radiance} < 8$
precision error of F_s^{rel} in the 772 nm window, P-polarization	$< 1\%$
outlier removal: F_s^{rel} in the 772 nm window, S-polarization	$-2.5\% < F_s^{rel} < 3.5\%$
land fraction	100%
average of out of band signal close to the bandpass filter	$< 1\%$
solar zenith angle	< 65 degree
$1.8 \cdot F_s^{rel}(771\,nm) - F_s^{rel}(755\,nm)$	$< 2.5 \cdot \sigma(F_s^{rel}(755\,nm))$

(755 nm and 772 nm) and 2 polarization directions (orthogonal P and S polarization spectra as recorded separately by GOSAT). The measurement noise estimates are derived from the standard deviation of the first and last 500 spectral samples of a GOSAT spectrum, both of which are outside the band pass filter and thus provide a realistic noise estimate on a spectrum-by-spectrum basis, since noise is white in an FTS spectrum.

Finally, the retrievals are filtered based on the goodness of the fit, retrieval precision as well as cloud contamination. Table S1 provides an overview of the applied post-processing filter criteria.

II. GOSAT INSTRUMENT

A. Zero level offset correction

In FTS systems, a detector signal non-linearity (either in the detector itself, in the preamplifier, or in the analog to digital converter(ADC)) can give rise to a zero level offset [1]. This has the same effect on Fraunhofer lines as chlorophyl fluorescence since both add signal in regions devoid of telluric absorption lines. The offsets caused by detection non-linearity depend on the peak interferogram signal level (roughly equivalent to the the average spectral signal). We notice that F_s^{rel} over Antarctica were non-zero and strongly correlated with the radiance level. Since no fluorescence is expected over ice, the spurious behavior of F_s^{rel} indicates a zero-level offset in GOSAT spectra. A further complication is that GOSAT uses two different gain settings. In order to correct the zero-level offset impact, we analyze fluorescence retrievals over regions with zero fluorescence but have to differentiate between the Gain settings, as the GOSAT instrument records spectra in two measurement settings, medium (M) and high (H) gain. For most regions, H-gain is applied but to avoid detector saturation, the lower gain setting (M) is used over the Sahara, parts of the Saudi-Arabian peninsula as well as central Australia. For the correction of M-gain spectra, we chose a region over the Sahara, which is devoid of vegetation (latitude:[18 30], longitude: [0 25]). For the correction of H-gain spectra, we chose Antarctica.

Figure S3 shows retrieved F_s^{rel} as well as average signal level of GOSAT spectra in the time period of December 2009 through February 2010. Owing to the large variation in solar zenith angles over this period, the average signal levels over Antarctica spans the full dynamic range of the detector despite an almost constant surface albedo. In the absence of continuum offset due to F_s or non-linearity, the fractional depths of Fraunhofer lines should be constant, independent of SZA or signal level. This enables us to characterize the zero-level offset based on spectra over Antarctica where no process should cause a solar zenith angle (SZA) dependent filling-in of Fraunhofer lines.

The left panel of figure S4 depicts the average of the retrieved offset (F_s^{rel}) as a function of averaged signal level for spectra over Antarctica. The two polarization directions as well as the two micro-windows show similar behavior, all exhibiting a systematic increase of F_s^{rel} with increasing signal level. The cause for the anomalous behavior of the curve at intermediate signal levels is so far not understood but probably due to ADC nonlinearity. The 4 curves are subsequently used to correct all H-gain retrievals (i.e. the value shown here given at the respective signal is subtracted). The right panel shows the standard deviation of the retrieved F_s^{rel} in the given signal level ranges.

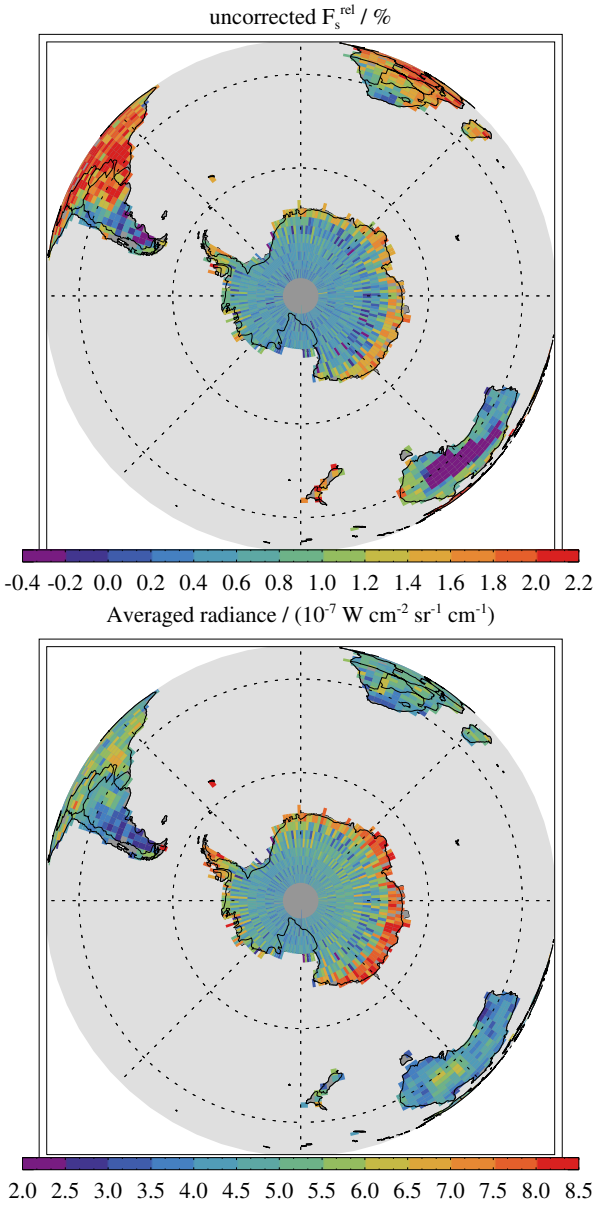

FIG. S3. Top: Retrieved raw F_s^{rel} in the southern hemisphere in December through February using S-polarization spectra and the 755 nm retrieval window. Bottom: Corresponding averaged radiances. Note the strong correlation between retrieved raw F_s^{rel} and average radiance over Antarctica. The gain setting change impact on F_s^{rel} can also be observed over the central part of Australia, which is commonly taken in gain M.

Since SNR increases with signal level, the standard deviation decreases systematically. The actual standard deviations agree with the expected ones, which are calculated from the posteriori covariance matrix of the weighted least-squares fit [2].

Figure S5 is similar to figure S4 but is based on M-gain spectra over the Sahara. Due to the

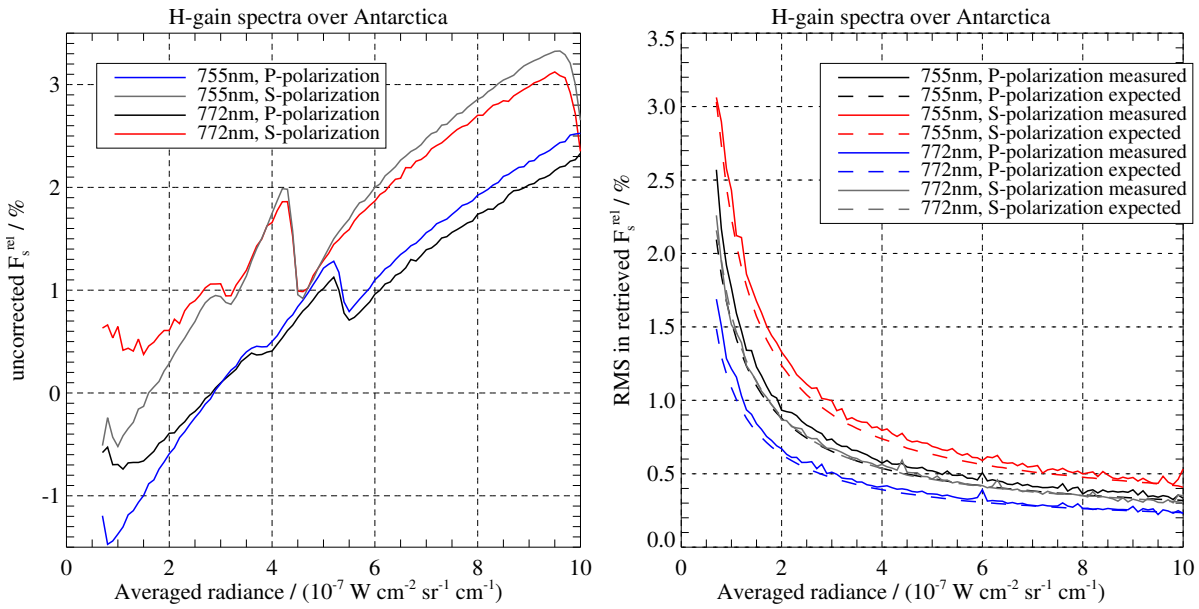

FIG. S4. Averaged retrieved raw F_s^{rel} as a function of averaged signal level using H-gain spectra over Antarctica. These curves are subsequently used to correct all H-gain spectra (treating the retrieval windows as well as polarization separately).

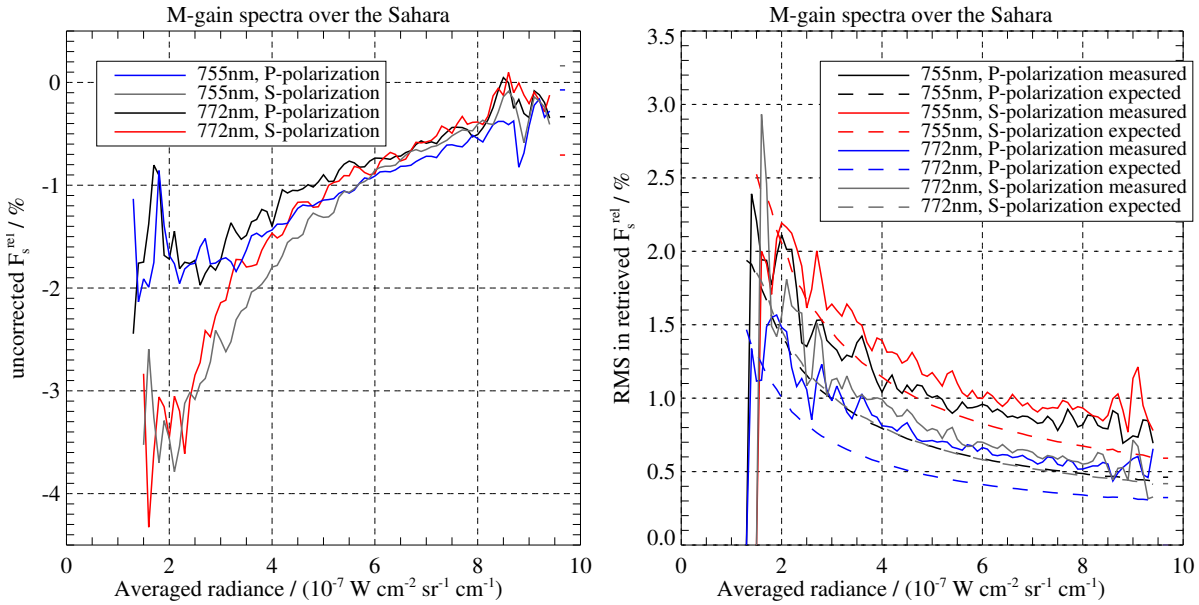

FIG. S5. Averaged retrieved raw F_s^{rel} as a function of averaged signal level using M-gain spectra over the central Sahara (latitude:[18 30], longitude: [0 25]). These curves are subsequently used to correct all M-gain spectra (treating the retrieval windows as well as polarization separately).

lower amount of spectra constituting the average, the noise in the curves is considerably larger. The behavior of the standard deviation (right panel) again closely follows the theoretical curves

but not as nicely as in the case of H-gain spectra. This may have to do with the occurrence of micro-vibrations disturbing M-gain interferograms, causing outliers in the fluorescence retrieval. Since this only affects M-gain spectra, which are mostly taken over deserts, it does not affect the analysis of the fluorescence signal over vegetation.

Further analysis showed that after correction, grid box averages of F_s based on retrievals using S-polarization spectra both over the Sahara and Antarctica are within $0 \pm 0.1 \mathrm{Wm}^{-2}\mu\mathrm{m}^{-1}\mathrm{sr}^{-1}$, irrespective of the time-period. F_s retrieved from P-polarization spectra is also about zero on average but still exhibits a significant time-dependence. Since the reason for this is currently unknown, P-polarization spectra are so far discarded in the further analysis and only the two micro-windows of the S-polarization spectra are used. The final average is constituted by the average of both retrieval windows but F_s at 772 nm is scaled with 1.8 prior to averaging (since the fluorescence emission spectrum is about 1.8 times higher at 755 nm compared to 772 nm).

B. Impact of the zero level offset correction on retrieved fluorescence

The correction for a zero level offset has a major impact on the retrieved signal. In fact, neglecting the zero level offset causes unphysical fluorescence values (strongly positive over bright surface such as Antarctica, Greenland or the Himalayas) and largely determines the variability of the signal (also because the radiance levels change with season, resulting in spurious seasonal cycles of retrieved fluorescence). This zero level offset effect was not included in the first fluorescence analysis of GOSAT spectra by Joiner *et al.* [4]. Figure S6 depicts the correction impact for an annual mean, separated for the 4 retrieval versions (2 windows, 2 polarizations). The location of regions where M-gain is used is well illustrated in the 771 nm/S-polarization panel (1st column, 2nd row). The Sahara, Arabian Peninsula, part of the Thar desert as well as the inner part of Australia exhibit negative retrievals and correspond exactly the location of M-gain measurements (having a different zero-level offset, hence a different retrieved signal).

After correction, the unexpected fluorescence signal over the deserts (taken with Gain H) such as Lut, Thar, Taklamakan, Kalahari or Atacama disappears and also spatial patterns change, indicating that the use of fluorescence retrievals without correction is fortuitous. The overall magnitude of the signal is also largely decreased, almost by a factor of 2. In addition, differences between Gain M and H are hardly discernible anymore, especially in S-polarization spectra. The most supportive evidence of a reliable correction scheme is now actually indicated by the contrast of the signal between the 755 and the 772 nm window. Before the correction, both windows indicated

fluorescence of similar magnitudes. After correction, however, the signal at 755 nm is about 80% higher than at 772 nm, in line with the strong negative slope of the fluorescence spectrum in this range.

Figure S7 shows the final corrected fluorescence signal in flux units (not as percent of the continuum signal). As noted before, the correction did not work perfectly for P-polarization spectra which is why we discarded those in the analysis performed in the main manuscript. The spatial patterns retrieved from S-polarization spectra, however, is very consistent and provides stable signals close to zero where expected.

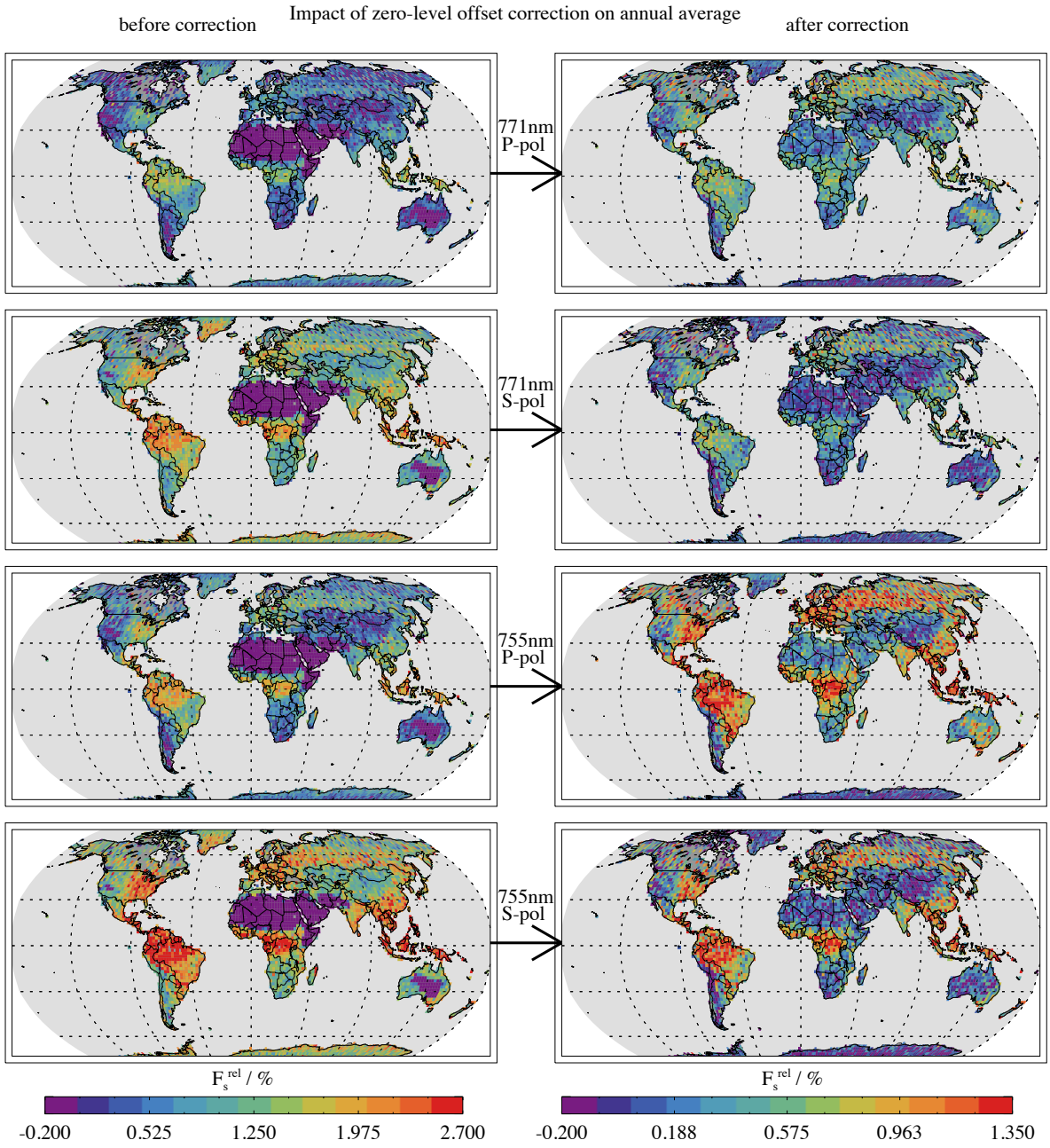

FIG. S6. Annual average of F_s^{rel} as defined in Frankenberg *et al.* [2] for the two polarization states and micro-windows before (left column) and after the empirical non-linearity correction (right column) outlined in the previous section. Note the different color-scales for corrected and uncorrected data. After correction, many bright but barren regions measured in gain H and not used for the determination of the correction (e.g. Himalayas, Rocky Mountains, Kalahari desert) are about zero, underlining the robustness of the approach.

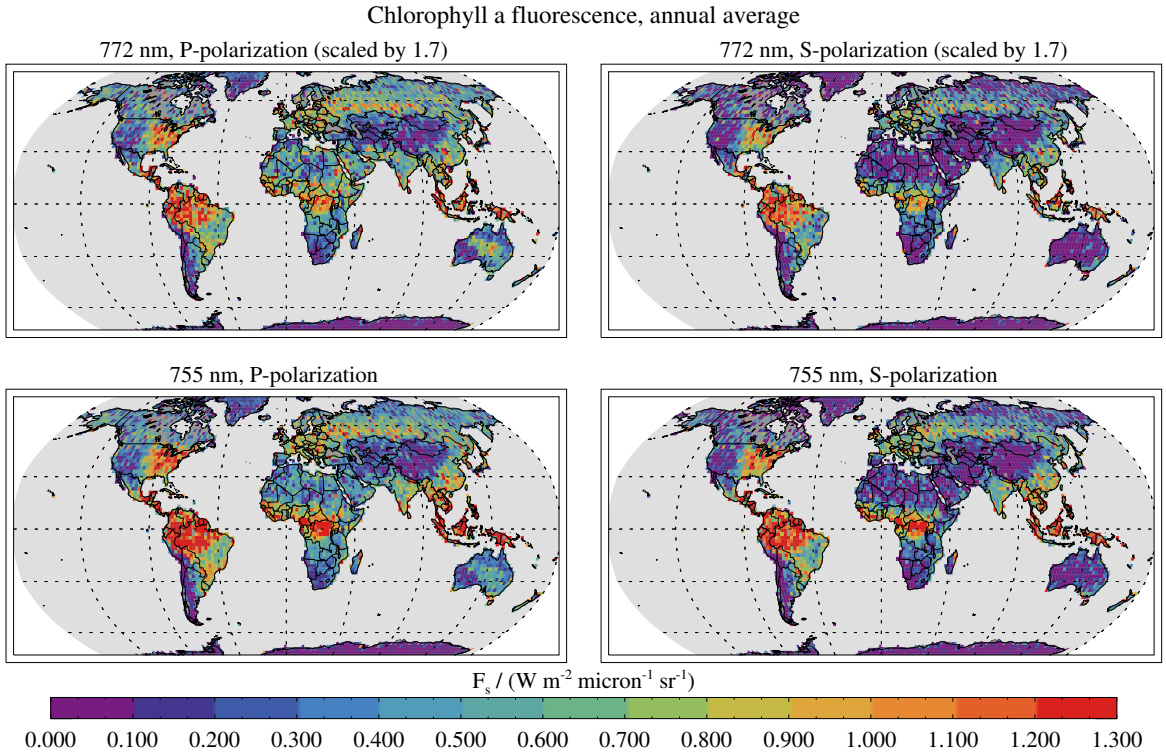

FIG. S7. Independent retrieval results of the annual average for the two different retrieval windows (755 and 772 nm) as well as the two polarization states. F_s from the 772 nm window has been scaled with 1.8 since the fluorescence emission in this window is already, as expected, considerably smaller than at 755 nm. Especially in regions where M-gain is used (Sahara, center of Australia), the P-polarization retrieval appears somewhat too high. This is consistent with our previous observations and P-polarization spectra are thus so far discarded in the results provided in the main document.

III. RETRIEVAL ACCURACY AND PRECISION ESTIMATES

The accuracy estimate derived from retrievals over Antarctica indicate systematic errors below $0.1\,\mathrm{Wm^{-2}}\mu\mathrm{m^{-1}sr^{-1}}$. In order to substantiate this finding, we retrieved fluorescence from purely ocean/sea soundings (where the oceanic chlorophyll content may impact the signal but to a much lesser degree than terrestrial vegetation). Figure S9 shows the annual average over the ocean gridded on 10°x10° (due to a lower amount of measurements passing the filter over the oceans, we had to perform a coarser gridding). Most retrieval, especially over ocean deserts, are within $\pm 0.1\mathrm{Wm^{-2}}\mu\mathrm{m^{-1}sr^{-1}}$ with a small overall low bias. Visual correlations with expected ocean chlorophyll content distributions are suggestive but outside the scope of this study.

Concerns that surface reflectance effects propagate into the final fluorescence retrieval can be discarded for the following reasons:

- Frankenberg *et al.* [2] show that the retrieved fluorescence can be disentangled from albedo effects.

- Considerable radiance changes are visible over Antarctica, Greenland, the Himalayas and over the ocean. Nevertheless, no systematic biases over these regions depending on signal level can be found.

- Fluorescence at 755 nm is, as expected, about 1.8 times higher than retrieved at 771 nm. If reflectance were a main cause of bias, it would affect both wavelengths in the same way and could not explain the observed difference.

- Fig.S8 clearly shows that regions with similar radiance (i.e. also reflectance), such as at the boundary of the Himalayas, show a stark contrast in fluorescence with no change in radiance levels. The same is true for many other regions (while for some vegetated areas, a correlation between F_s and radiance is expected as radiance at 760nm correlates with NDVI).

Based on the discussion in this section, we provide a conservative accuracy estimate of $\pm 0.15\,\mathrm{Wm^{-2}}\mu\mathrm{m^{-1}sr^{-1}}$.

The estimated statistical noise (precision error) on a single retrieval is on the order of 0.5% of the continuum radiance. In order to improve the precision, as many soundings as possible have to be averaged. Figure S10 shows the the standard error of the weighted average of F_s as shown in Figure 1 in the main text. Precision errors provided elsewhere are calculated accordingly. As we

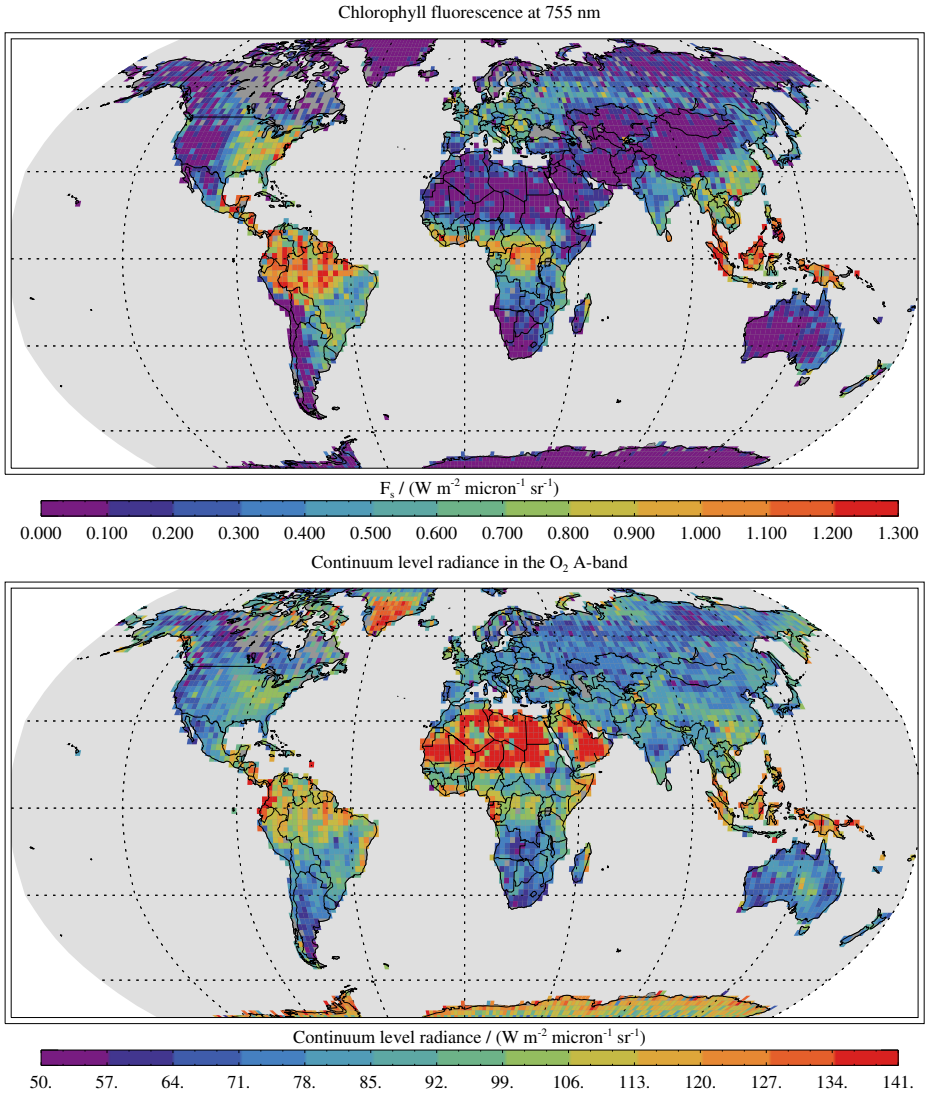

FIG. S8. Fluorescence (top) and continuum level radiance (bottom) annual average.

have seen that the actual standard deviation of retrievals over Antarctica corresponds well to the theoretical one, we consider our precision estimate robust.

IV. DERIVATION OF DAILY FLUORESCENCE AVERAGES FROM INSTANTANEOUS MEASUREMENTS

Especially at high latitudes, the fluorescence signal at overpass time cannot be directly compared with GPP since a) local overpass time may deviate slightly from 13:00 and b) the length of day and variability of the solar zenith angle has to be taken into account. Under cloud-free conditions and ignoring Rayleigh scattering as well as gas absorption, the downwelling solar radiation scales

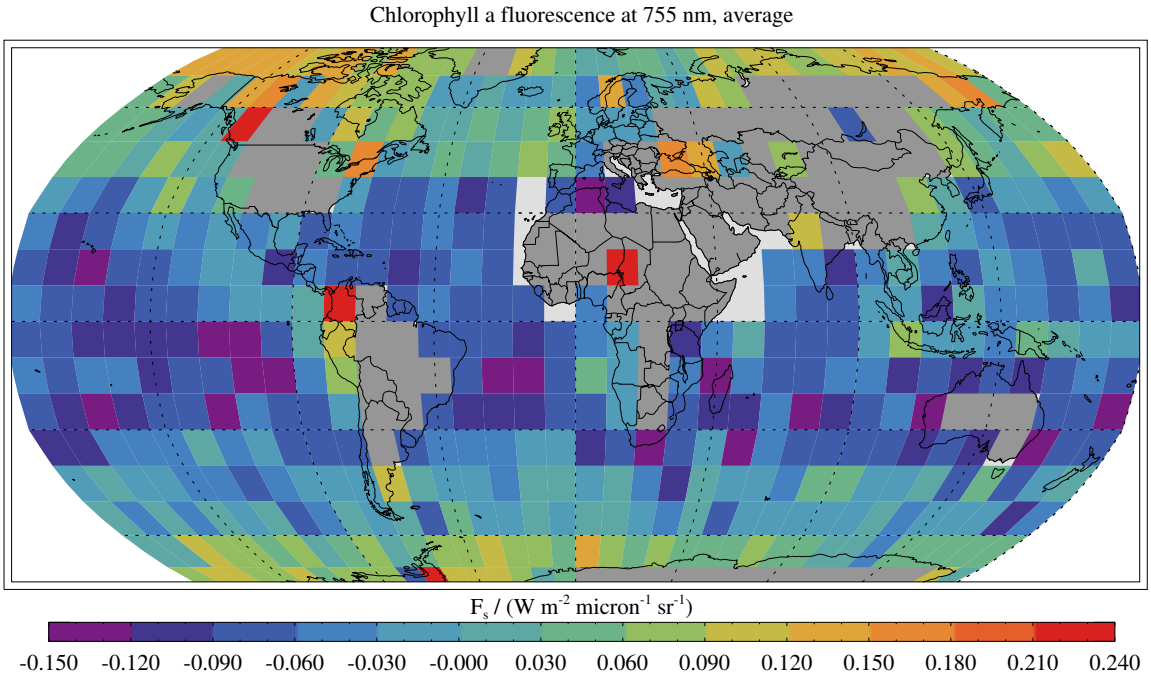

FIG. S9. Average of all S-polarization spectra with 0% land cover gridded on 10°x10°. The 772 nm retrievals have been scaled by 1.7 prior to averaging with the 755 nm retrievals. Please note the far smaller range of the color-scale (as compared to land-only data). In general, variability is very low and lowest retrievals are observed over the ocean desert. Visual correlations with ocean chlorophyll contents are suggestive but a detailed analysis is beyond the scope of the current study. Some pixels over landmasses exist and are most likely related to 0% land cover owing to large water bodies. However, geolocation mismatches may mix vegetation into these signals, causing higher values.

linearly with $\cos(SZA)$. If t_0 denotes the time of measurement in fractional days, a first order approximation for a daily fluorescence average can be written as:

$$\overline{F_S} = F_s / \cos(SZA(t_0)) \cdot \int_{t=t_0}^{t=t_0+1} \cos(SZA(t))dt$$

The aforementioned correction has been applied to each individual GOSAT sounding, computing the integral numerically in 10 minute time-steps (Using pyEphem (http://rhodesmill.org/pyephem/) to compute SZA as a function of latitude, longitude and time). Apart from a reduction in the absolute F_s value by a factor 3 (as a daily average is calculated from a noon measurement at its daily maximum), the correction has very little effect at low latitudes but increases towards higher latitudes. Figure 3 of the main text provides both, F_s and scaled $\overline{F_S}$.

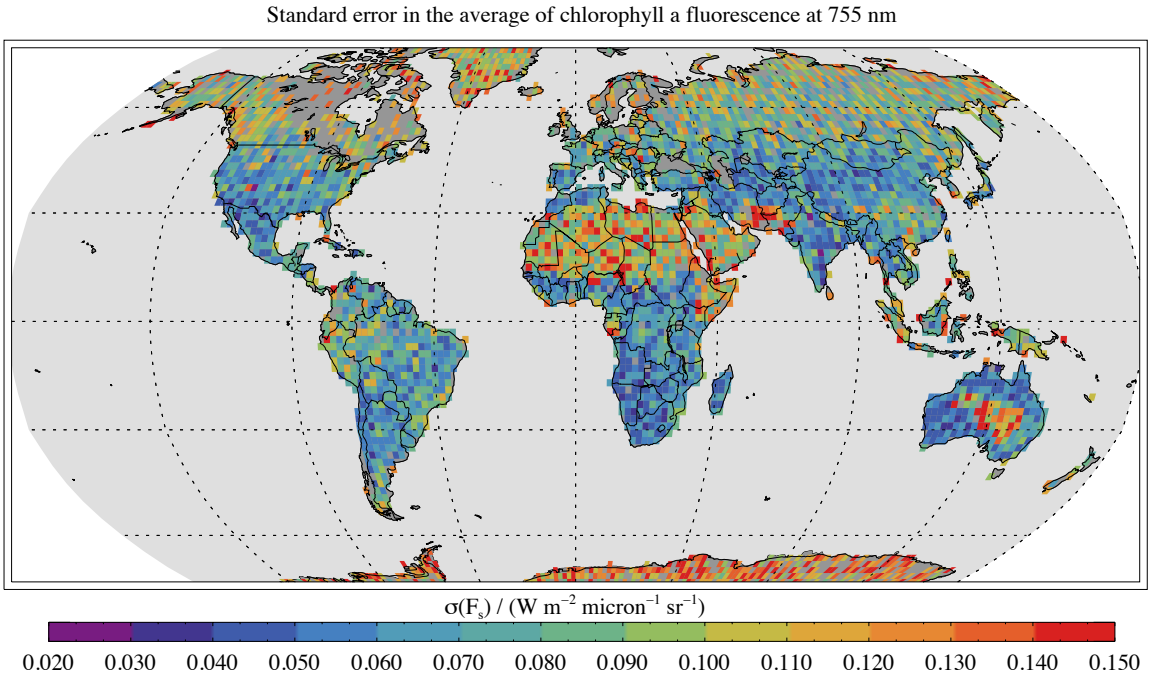

FIG. S10. Standard error of the weighted average of F_s, computed as $\sigma_{\overline{F_s}} = \sqrt{\left(\frac{1}{\sum_{i=1}^{n}(1/\sigma_i^2)}\right)}$, with n denoting the number of soundings averaged per grid cell (both P and S-polarization) and σ_i their respective 1σ precision errors. Peak values of F_s are $\approx 1.2\mathrm{Wm}^{-2}\mu\mathrm{m}^{-2}\mathrm{sr}^{-1}$, so the standard errors plotted above are 5-10% of the peak F_s.

V. RELATIONSHIP BETWEEN GPP, LUE AND FLUORESCENCE

Gross primary production is the product of light use efficiency (yield of photosynthesis) and absorbed photosynthetic active radiation

$$GPP = LUE \cdot APAR\,. \tag{1}$$

Similarly, the absolute value of fluorescence emission is

$$F_s = \phi_{F_s} \cdot APAR\,, \tag{2}$$

with ϕ_{F_s} denoting the fluorescence yield. An implicit correlation of F_s with GPP exists trough the relationship of both with $APAR$. If the ratio of LUE and ϕ_{F_s} remains unchanged, F_s is strictly proportional to GPP. It is well established that fluorescence and photosynthesis yield at low light intensities are anti-correlated. At high light intensities, however, they are positively correlated because with increasing irradiance and moisture stress, chlorophyll fluorescence and photochemistry both drop by the same factor due to deactivation of antennae to prevent damage by harmful radicals [6, and references therein]. Since GOSAT measures at 13:00 local time, high

light intensities can be assumed and this is probably the reason for the excellent correspondence of F_s with GPP. However, it should also be mentioned that APAR derived from MODIS indices can also be erroneous and that the direct correlation of F_s with *true* APAR helps improve the correlation with GPP. We acknowledge that further studies are needed to understand the complex fluorescence signal on regional scales, for different biomes and varying conditions.

VI. MODIS ANALYSIS

When comparing with Terra MODIS data, we calculate exact single-sounding coincidences with MODIS before performing any averaging on coarser grid boxes. This way, we avoid any sampling error due to incomplete global coverage of GOSAT.

We processed the following datasets from the MODIS 5 Land Collection::

- MOD13A2 Terra Vegetation Indices Tile 1000m 16 Day
- MOD15A2 Terra Leaf Area Index - FPAR CMG 5600m 8 Day
- MOD17A2 Terra Gross Primary Productivity Tile 1000m 8 Day

Our analysis included a separate MOD17A2 and MOD15A2 with improvements described in Zhao *et al.* [7]. The particular version of the MODIS GPP product we are using is identical to Zhao and Running [8]. Since this dataset was not available for 2010, we used 2009 data for the months in 2010 as well (not affecting the JJA discrepancies as those were calculated only for 2009). All other MODIS data is exactly matching the fluorescence retrievals in time and space.

A. Methods

After filtering each MODIS pixel for quality assurance (described below), we averaged together the remaining valid MODIS pixels to arrive at a single MODIS value for each single GOSAT sounding. Each GOSAT pixel covers a circular area, with a radius of 5 km. Each MODIS pixel is 1 km by 1 km. For each GOSAT pixel, we extracted all MODIS pixels with a center point that fell within 5 km of the center point of the GOSAT pixel. MODIS pixels partially falling into the GOSAT footprint, the center of which lay outside the 5 km radius were not included. Because the MOD17A2 product reports the cumulative amount of GPP per composite period (typically 8 days), we divided the final GPP value by the length of the composite period to get daily GPP values. The MOD15A2 product was provided as a globally gridded 0.05 degree dataset, with each

pixel representing an average of the underlying 1km MODIS pixels. For each GOSAT pixel, we selected the one 0.05 LAI pixel with the greatest degree of overlap with the GOSAT footprint.

B. Quality assurance

MODIS data comes with pixel by pixel quality assurance flags. We outline the filter scheme used for each MODIS product here:

MOD13 comes with two general quality indicators on bits 0-5. We excluded all data deemed 'most probably cloudy' and pixels with a VI usefulness score of 'Lowest Quality' or below. On bits 6-7, we excluded all pixels with an Aerosol quantity score of 'High'. Finally, on bit 15, we excluded data with covered in shadows. Documentation for MOD13 QA found here: `https://lpdaac.usgs.gov/lpdaac/products/modis_products_table/vegetation_indices/16_day_l3_global_1km/mod13a2`

MOD15: LAI On bit 2 of the General FPAR/LAI QA field, we excluded all pixels with a 'Dead Detector.' On bit 3-4, we excluded all pixels with 'Mixed cloud' and 'Significant clouds'. Furthermore, if the cloud state was not defined, we excluded those pixels as well. On bit 6 of the Detailed FPAR/LAI QA field, we excluded all pixels with cloud shadow. Documentation on MOD15 QA found here: `https://lpdaac.usgs.gov/lpdaac/products/modis_products_table/gross_primary_productivity/8_day_l4_global_1km/mod17a2`

MOD17 The Zhao/Running version of the MOD17 product comes with no QA fields, as all necessary filtering takes place within their correction process. See Zhao *et al.* [7] for details.

When GOSAT data is averaged within a grid box, we only consider MODIS data when at least 10 valid MODIS pixels fall within a GOSAT footprint (a stricter criterion would filter almost all tropical MODIS data).

VII. ADDITIONAL PLOTS

A. Seasonally dependent scatterplots

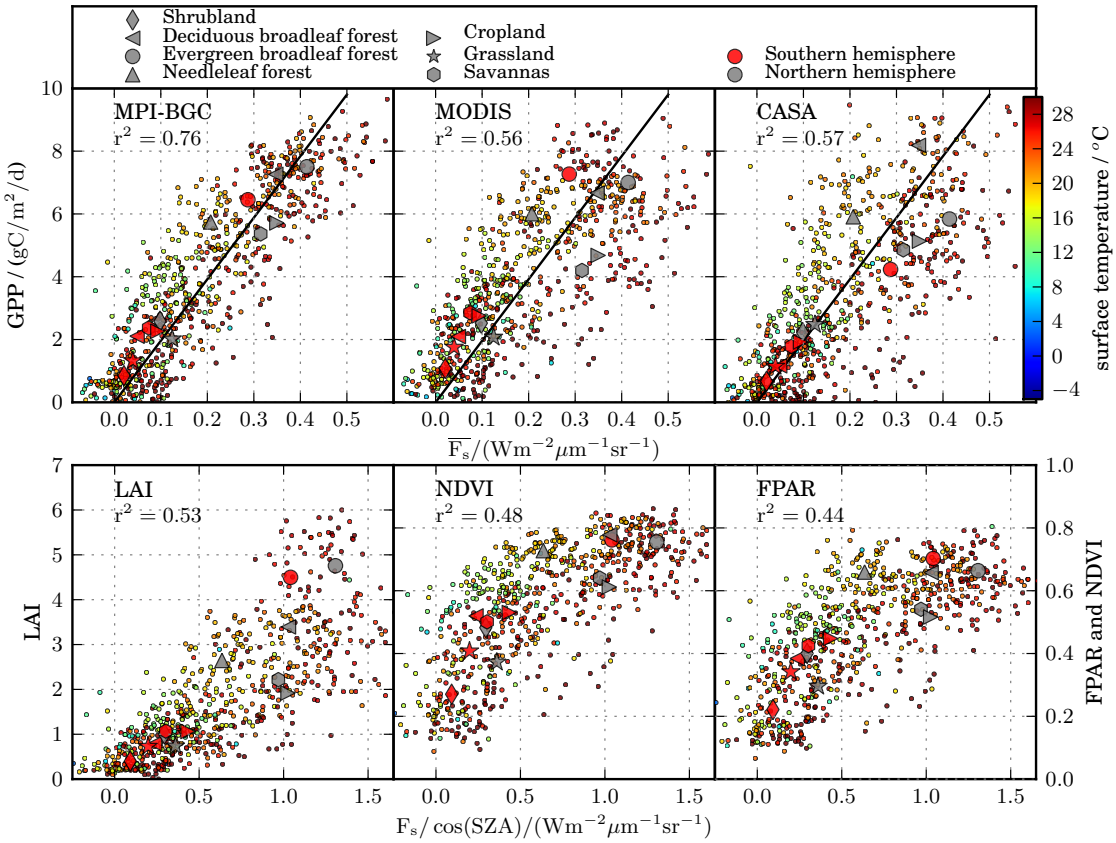

FIG. S11. Scatterplot as in Fig. 2 of the main text but separately for June through August (JJA)

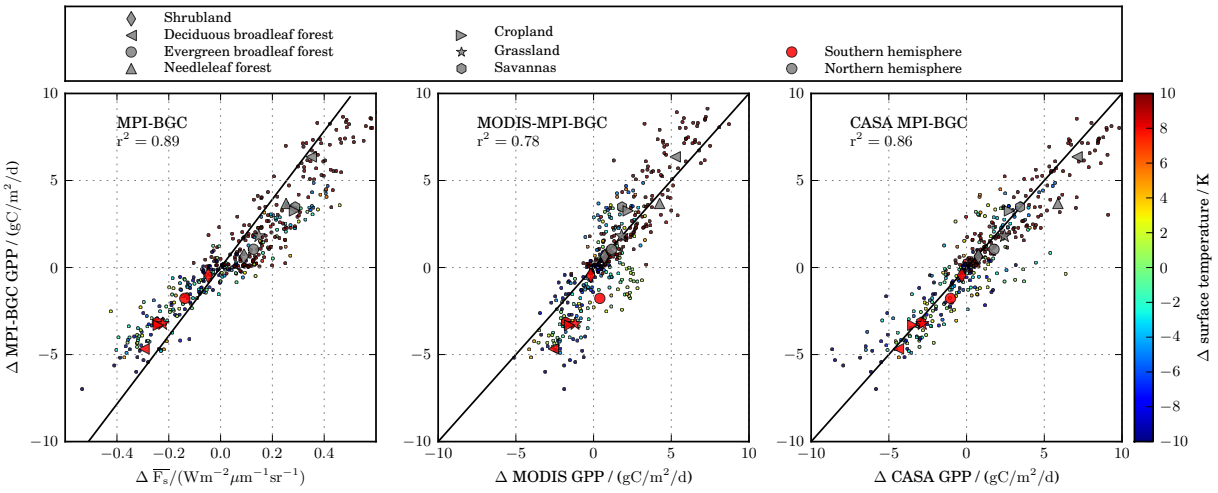

FIG. S12. Correlation plot for the seasonal amplitude (difference between JJA and DJF) of Fscorr vs. MPI-BGC GPP, MODIS GPP vs. MPI-BGC GPP and CASA GPP vs. MPI-BGC GPP. As the calculation requires grid box averages of F_s in both seasons, high latitudes (above approx. 50°N) are not included in the analysis as low solar zenith angles in winter impede the retrieval. It can be seen that some areas experience an increase in GPP despite a reduction in surface temperature. Especially MODIS seems to underestimate these effects.

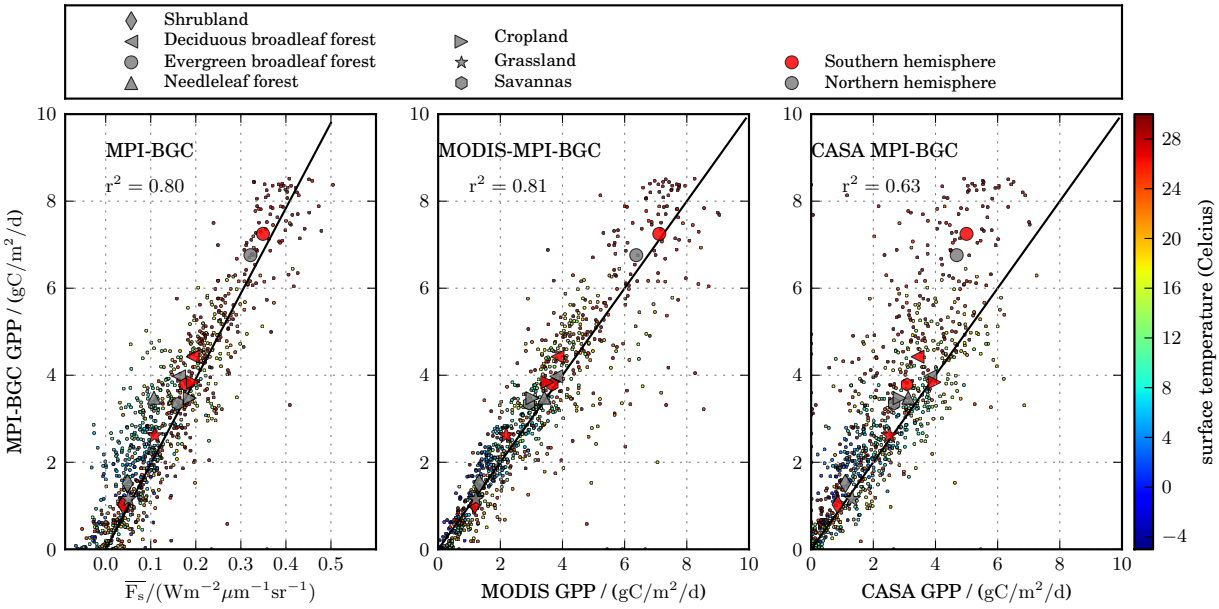

FIG. S13. Correlation plot for the annual average (as Fig. 2) of $\overline{F_S}$ vs. MPI-BGC GPP, MODIS GPP vs. MPI-BGC GPP and CASA GPP vs. MPI-BGC GPP. ECMWF surface temperature is color-coded for each 4x4 degree grid box average.

B. Spatially explicit differences in boreal summer

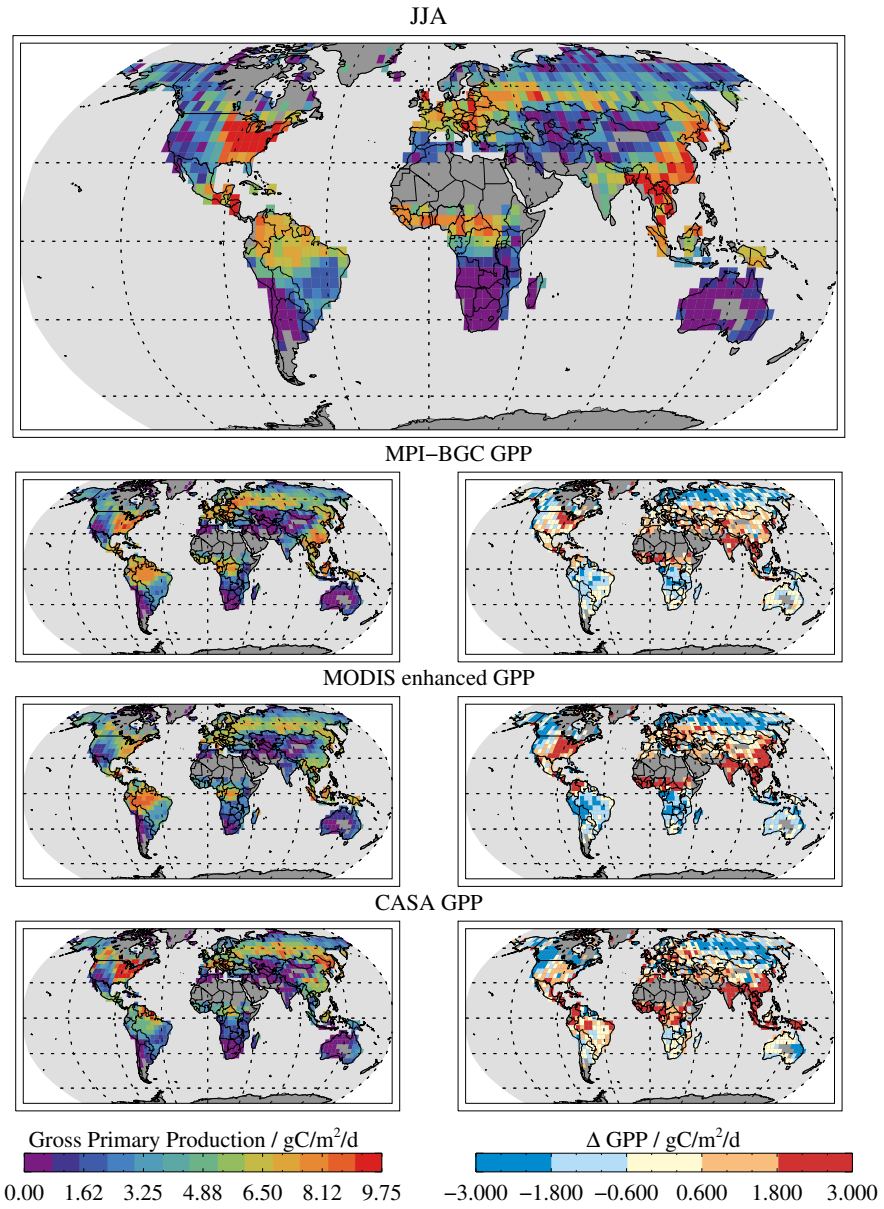

FIG. S14. Top panel: JJA GPP derived from the approximated linear relationship with F_s. Small panels, left side: Individual GPP panels for the same time period; right side: difference with respect to the fluorescence estimate. The most robust differences when compared to all models are found in African savannas and in Asia. Most other regions display varying patters in the respective models (e.g. US croplands are more consistent with CASA than with MPI-BCG and MODIS).

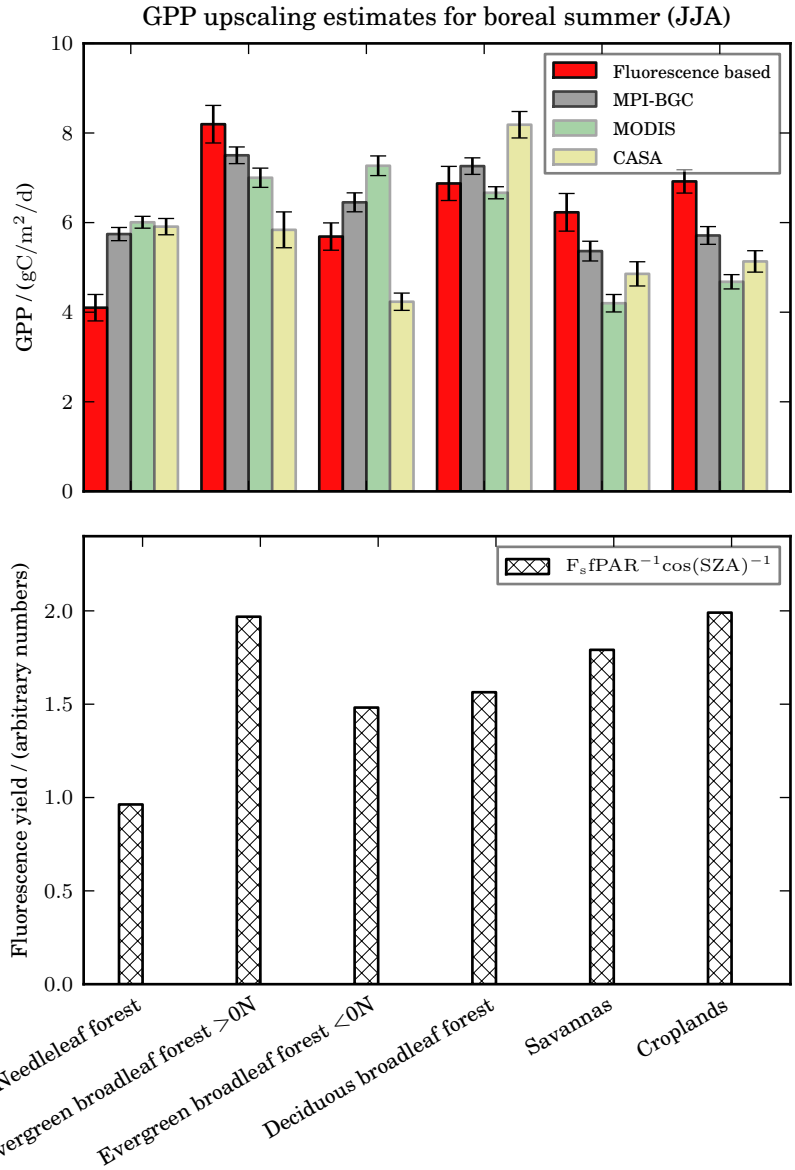

FIG. S15. Chlorophyll fluorescence based GPP estimate (using the simple empirical linear relationship) and comparison with model GPP estimates for the most important biomes in the northern hemisphere in the growing season. An empirical GPP based on fluorescence is calculated from the slope of the linear fit with the MPI-BGC GPP in the annual average (see Fig. 2). For needleleaf forest, fluorescence based GPP is 28-32% lower than model estimates while it is 18-48% higher for savannas and croplands. Error bars indicate the 95% confidence interval of the average of all 1x1 degree grid boxes constituting the biome average (standard deviation derived from the true standard deviation of all grid-boxes). The lower panel shows the ratios of F_s (normalized by cos(SZA)) with fPAR, being directly proportional to the fluorescence yield. The observed high variability among different biomes is broadly consistent with an analysis of LUE at some flux tower sites (Turner et al, 2003).

C. Biome classification

We adopted the ISLSCP Initiative II biome classification on 1x1 degree resolution to aggregate soundings by biome: Friedl, M.A., A.H. Strahler, and J. Hodges (2010), ISLSCP II MODIS (Collection 4) IGPB Land Cover, 2000-2001. In Hall, Forest G., G. Collatz, B. Meeson, S. Los, E. Brown de Colstoun, and D. Landis (eds.). ISLSCP Initiative II Collection. Data set. Available on-line [http://daac.ornl.gov/] from Oak Ridge National Laboratory Distributed Active Archive Center, Oak Ridge, Tennessee, U.S.A. doi:10.3334/ORNLDAAC/968.

For simplification, we combined some IGBP classes:

- Evergreen and deciduous needleleaf forests (class 1 and 3) are combined into *needleleaf forest*
- Deciduous Broadleaf Forests and Mixed forests (class 4 and 5) are combined into Deciduous Broadleaf Forests (as Deciduous Broadleaf Forests constitutes the largest area)
- Closed and Open Shrublands are combined into *Shrublands*
- Woody Savannas and Savannas are combined into *Savannas*
- Croplands and Cropland/Natural Vegetation Mosaic (classes 12 and 14) are combined into *Croplands*

Figure S16 depicts the geographical distribution of the 7 biomes used in the main text of the manuscript.

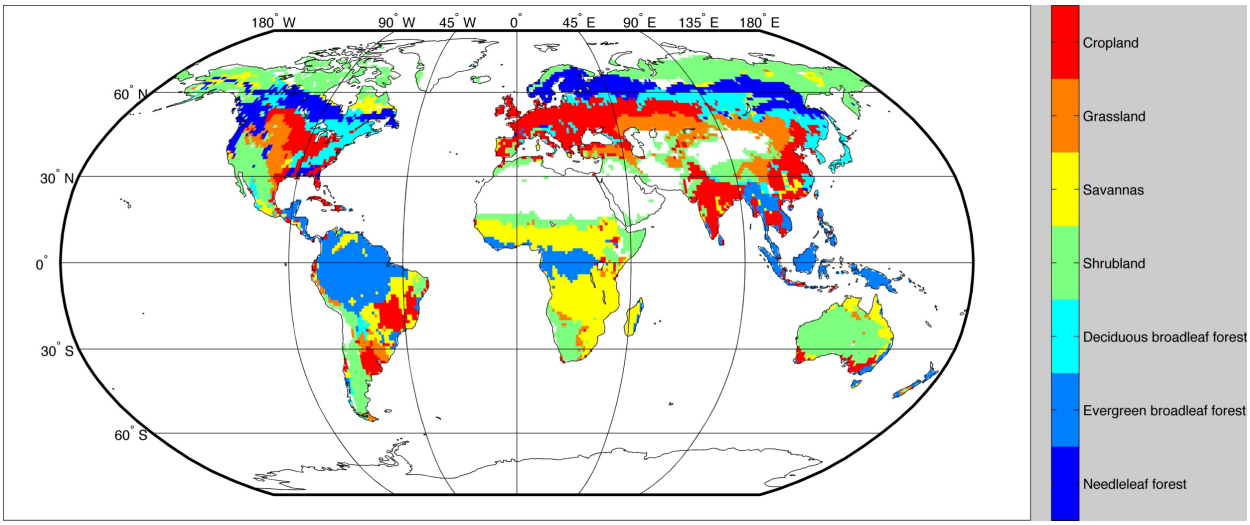

FIG. S16. Biome classification.

[1] Abrams, M., G. Toon, and R. Schindler, 1994 Jan, Appl. Opt. http://www.opticsinfobase.org/abstract.cfm?URI=ao-33-27-6307.

[2] Frankenberg, C., A. Butz, and G. Toon, 2011, Geophys. Res. Let. **38** (3), L03801, ISSN 0094-8276.

[3] Frankenberg, C., U. Platt, and T. Wagner, 2005, Atmos. Chem. Phys **5**, 9.

[4] Joiner, J., Y. Yoshida, A. Vasilkov, Y. Yoshida, L. Corp, and E. Middleton, 2010 Nov, Biogeosciences Discuss. **7** (6), 8281, http://www.biogeosciences-discuss.net/7/8281/2010/.

[5] Kauppinen, J., and P. Saarinen, 1992, Appl. Opt. **31** (1), 69.

[6] Van der Tol, C., W. Verhoef, and A. Rosema, 2009, Agricultural and Forest Meteorology **149** (1), 96, ISSN 0168-1923.

[7] Zhao, M., F. Heinsch, R. Nemani, and S. Running, 2005, Remote sensing of Environment **95** (2), 164, ISSN 0034-4257.

[8] Zhao, M., and S. Running, 2010, Science **329** (5994), 940.